Materials Today Bio 23 (2023) 100882

Contents lists available at ScienceDirect

Materials Today Bio

journal homepage: www.journals.elsevier.com/materials-today-bio

Photo-crosslinked bioactive BG/BMSCs@GelMA hydrogels for bone-defect repairs

Yufeng Ai [a,b,c,e,1], Fang Dai [a,b,c], Wenfeng Li [a,b,c], Fancheng Xu [a,b,c,e], Hanwen Yang [e], Jianxin Wu [a,b,c,e], Kaiqiang Yang [a,b,c,e], Li Li [a,b,c,e], Fanrong Ai [d,**], Li Song [a,b,c,*]

[a] Center of Stomatology, The Second Affiliated Hospital of Nanchang University, Nanchang, Jiangxi, 33006, China
[b] The Institute of Periodontal Disease, Nanchang University, Nanchang, Jiangxi, 33006, China
[c] JXHC Key Laboratory of Periodontology (The Second Affiliated Hospital of Nanchang University), Nanchang, Jiangxi, 33006, China
[d] School of Advanced Manufacturing, Nanchang University, Nanchang, Jiangxi, 33006, China
[e] The Second Clinical Medical School, Nanchang University, Nanchang, Jiangxi, 33006, China

ARTICLE INFO

Keywords:
GelMA
BMSCs
Bio-active glass
Bone regeneration

ABSTRACT

The clinical treatments of bone defects remain a challenge. Hydrogels containing bone marrow mesenchymal stem cells (BMSCs) are extensively used to bone regeneration because of excellent biocompatibility and hydrophilicity. However, the insufficient osteo-induction capacity of the BMSC-loaded hydrogels limits their clinical applications. In this study, bio-active glass (BG) and BMSCs were combined with gelatin methacryloyl (GelMA) to fabricate composite hydrogels via photo-crosslinking, and the regulation of bone regeneration was investigated. In vitro experiments showed that the BG/BMSCs@GelMA hydrogel had excellent cytocompatibility and promoted osteogenic differentiation in BMSCs. Furthermore, the BG/BMSCs@GelMA hydrogel was injected into critical-sized calvarial defects, and the results further confirmed its excellent angiogenetic and bone regeneration capacity. In addition, BG/BMSCs@GelMA promoted the polarization of macrophages towards the M2 phenotype. In summary, this novel composite hydrogel demonstrated remarkable potential for application in bone regeneration due to its immunomodulatory, excellent angiogenetic as well as osteo-induction capacity.

Credit author statement

Li Song and Fanrong Ai designed the study. Yufeng Ai conducted experiments. Fang Dai, Wenfeng Li and Fancheng Xu performed data analysis. Hanwen Yang, Jianxin Wu, Kaiqiang Yang and Li Li collected the experimental data. Li Song, Fanrong Ai and Yufeng Ai wrote and revised the manuscript.

1. Introduction

Bone defects are often caused by periodontitis, trauma, osteoporosis, tumours, and osteoarthritis, which negatively affect the quality of life [1]. The repair of critical bone defects usually requires transplantation. The materials used for bone-defect repairs include autologous bone, allogeneic bone, xenogenic bone, metal, and ceramic materials. However, the application of bone graft materials is limited by an insufficient number of transplanted bones, rejection reactions, and limited osteogenic capabilities. Currently, there are no ideal bone-graft materials [2].

The extracellular matrix (ECM) regulates the biological behaviour of cells [3]. Therefore, biomaterials should control cell proliferation and differentiation by emulating the ECM to promote tissue regeneration. Because the main components of the ECM are proteoglycans and proteins, bone graft materials based on natural proteins and polysaccharides have received widespread attention [4]. GelMA prepared by the reaction of gelatin with MA contains arginine-glycine-aspartate (RGD) sequence and matrix metalloproteinase (MMP), which can promote cell adhesion, proliferation and differentiation [5]. Simultaneously, GelMA can permanently fix the shape of the hydrogel through covalent crosslinking subjected to ultraviolet (UV) light exposure to compensate for the shortcomings in the mechanical properties of gelatin [6]. These characteristics make GelMA extensively used in tissue engineering research, including bone, cartilage, blood vessels, and the heart

* Corresponding author. Center of Stomatology, The Second Affiliated Hospital of Nanchang University, Nanchang, Jiangxi, 33006, China.
** Corresponding author.
E-mail addresses: afr3755875@126.com (F. Ai), ndefy91009@ncu.edu.cn (L. Song).
[1] First author.

https://doi.org/10.1016/j.mtbio.2023.100882
Received 2 September 2023; Received in revised form 5 November 2023; Accepted 22 November 2023
Available online 6 December 2023

Table 1
The developed hydrogels and their chemical compositions.

GelMA	GelMA	BG
	5 % (w/w)	—
0.5%BG@GelMA	5 % (w/w)	0.5 % (w/w)
1.0 % BG@GelMA	5 % (w/w)	1.0 % (w/w)
1.5 % BG@GelMA	5 % (w/w)	1.5 % (w/w)
2.0 % BG@GelMA	5 % (w/w)	2.0 % (w/w)

[7–10].

Bone marrow stromal cells (BMSCs) were first identified by Friedenstein in 1976. BMSCs participate in tissue repair and mediate immune responses through cell differentiation and paracrine mechanisms in specific environments [11–13]. Currently, the major way of stem cell therapy involves the injection of stem cells directly into the treatment region, thereby reducing the damage caused by surgery. However, the low-retention rate of the injected BMSCs and the complex microenvironment of the implant area limit cell proliferation and differentiation, which are important barriers to effective clinical translation. To solve this problem, many researchers have encapsulated cells in hydrogels to provide a stable microenvironment conducive to cell proliferation and differentiation [14]. In recent years, GelMA hydrogels containing RGD- and MMP- target sequences have attracted widespread research attention. However, because the osteogenic capability of the GelMA hydrogel is limited [15], the osteo-inductive capability of the GelMA-BMSC hydrogel cannot be guaranteed. Therefore, various polymers, bio-macromolecules, and nano-materials have been introduced into GelMA hydrogel [2,16,17]. For example, Chai et al. [18] wrapped BMSCs and BMP-2 in photo-crosslinkable GelMA, in which BMSCs exhibited enhanced osteogenic effects. Li et al. [19] showed that hydrogel containing deferoxamine can promote angiogenesis and bone regeneration. However, inflammation and heterotopic bone regeneration caused by the high-dose release of BMP-2 limit the application of these materials [20].

Compared with growth factor release, the advantage of bio-glass in promoting bone regeneration is not only its lower cost but more importantly the fact that ions released by bio-glass are easier to control [21]. A single ion can activate a specific cellular response that requires the precise delivery of large amounts of growth factors [22–24]. In addition, the activity of growth factors is limited by their half-lives in the body as well as the micro-environment. 45S5 bio-glass (BG) is one of the third-generation bio-active inorganic materials and has been extensively studied and applied to bone-defect repair and wound repair [25,26]. 45S5 BG can form a hydroxyapatite layer at the interface between the material and bone defect, which can firmly bind BG to living bone and tissue [27]. Second, 45S5 BG triggers and enhances cellular activity during tissue regeneration via its dissolved products [28]. Third, new blood vessels in the body deliver oxygen and nutrients to surrounding tissues to promote survival and growth [29], maintain the internal homeostasis of bone tissue, and promote the differentiation of BMSCs to osteoblasts, thus promoting bone regeneration. Study have shown that 45S5 BG promotes the vascularization of endothelial cells [30]. Compared with the short half-life and high price of cytokines, BG has great advantages in practical application. Studies have shown that BG ion products regulate exosome secretion from BMSCs. For example, BG ions downregulate micro-ribonucleic acid (miR)-342-5p and upregulate miR-1290 in MSCs, thereby promoting endothelial cell vascularization [25]. The degradation product of BG is hydroxyapatite, which is one of the main components of natural bone and teeth. Adding BG to the GelMA hydrogel makes it more similar to the ECM of natural bone. After BMSC encapsulation, a micro-environment similar to that of the ECM in the hydrogel was conducive to the proliferation of BMSCs, and addition of BG promoted bone regeneration in situ by inducing the osteogenic differentiation of BMSCs.

Immune cells play an important role in bone tissue regeneration [31]. Among these cells, macrophages have gained widespread attention for their important role in regulating multiple stages of bone tissue

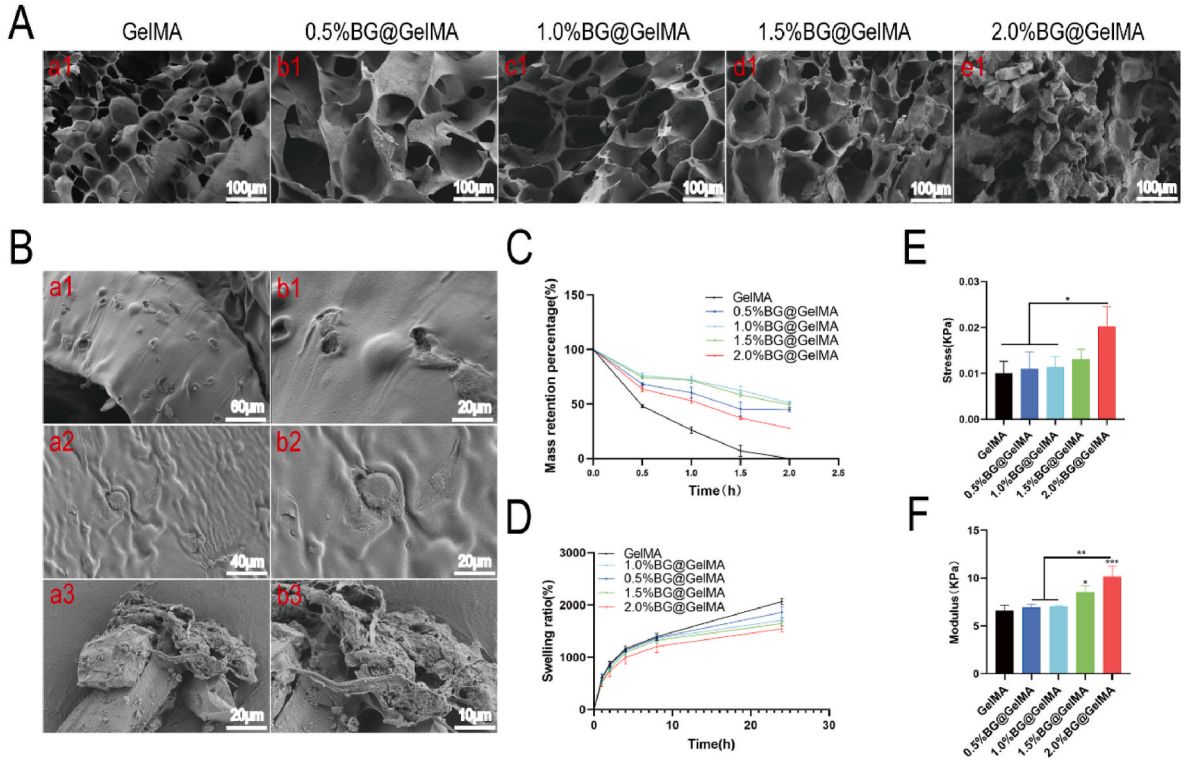

Fig. 1. Characterization of hydrogels. (A) Cross-section image of hydrogel (SEM). (B) SEM images in the different groups. (C) Degradation properties of GelMA and BG@GelMA hydrogel in vitro. (D) Dynamic swelling behaviors of GelMA and BG@GelMA hydrogel in vitro. (E) Stress when the hydrogel strain reaches 50 % after UV crosslinking. (F) The compressive modulus of hydrogels after UV crosslinking. The data presented as mean ± SD, n = 3. $^{*}P < 0.05$, $^{**}P < 0.01$ and $^{***}P < 0.001$.

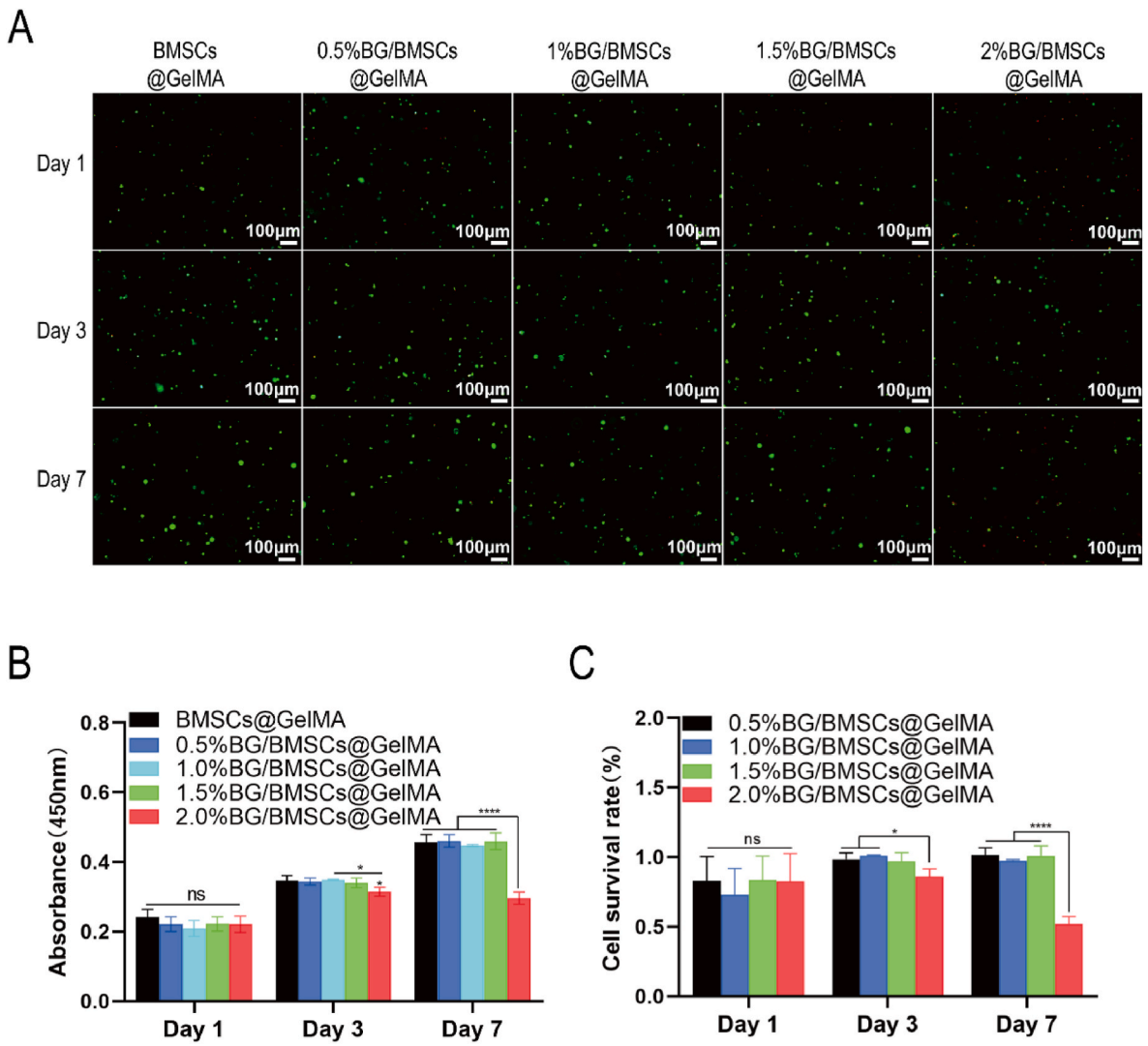

Fig. 2. In vitro evaluation of the cytocompatibility of the hydrogel. (A) Calcein-AM/PI staining. (B) Proliferation of BMSCs in different hydrogels. (C) Cell survival rate. Data presented as mean ± SD, n = 4. *$P < 0.05$, ****$P < 0.0001$.

repair [32,33]. Macrophages were divided into proinflammatory M1 phenotype and anti-inflammatory M2 phenotype [34]. M1 macrophages are involved in phagocytosis and early angiogenesis by releasing pro-inflammatory signals in bone defect repair. However, the long-term presence of M1 macrophages induces chronic inflammation and inhibits tissue healing [35]. Therefore, inducing the transformation of M1 macrophages into M2 phenotypes in bone tissue is a promising innovative strategy for bone defect repair. Many bioactive ions have been shown to affect the recruitment, maturation, activation, and secretion of pro-inflammatory and anti-inflammatory cytokines in macrophages [36,37]. BGs have been considered to be an effective platform for releasing bioactive ions that promote the transformation of M1 macrophages into M2 phenotypes [38,39]. However, the underlying mechanism has not been fully elucidated, but it has been reported that it is involved in the Toll-like receptor (TLR) pathway and the activation of NF-κB [35]. Therefore, in our strategy, the addition of BG promotes vascular regeneration, induce the polarization of M1 macrophages towards M2 phenotype, promotes bone regeneration.

In the present article, we designed a hydrogel that contained BMSCs and 45S5BG. To confirm our hypothesis, we first optimised the concentration of loaded BG in the GelMA hydrogel and then investigated the proliferation and differentiation of MSCs encapsulated in GelMA. The hydrogels exhibited good mechanical properties and bio-compatibility. In vitro experiments showed that adding BG to the BMSCs@GelMA hydrogel could further endow the hydrogel with the desired osteoinductive properties. In addition, this study confirmed the excellent bio-compatibility, angiogenetic, immunomodulatory and osteogenic functions of the composite hydrogel based on micro-computed tomography (micro-CT), hematoxylin & eosin (H&E), Masson's trichrome, immunofluorescence staining in a Sprague–Dawley rat cranial-defect model.

2. Method

2.1. Materials

GelMA was obtained from SunP Biotech (Beijing, China). Lithium phenyl (2,4,6-trimethylbenzoyl) phosphinate (LAP), propidium iodide, calcein-acetoxymethyl, GelMA lysis solutions were purchased from EFL (Suzhou, China). Cell counting kit-8 (CCK-8) was obtained from Yeasen Biotechnology (Shanghai, China). Trypsin, penicillin–streptomycin, Dulbecco's modified eagle's medium (DMEM)/F12 were purchased from Service Bio (Wuhan, China). Foetal bovine serum (FBS) was obtained from CellMax (Shanghai, China). The BG was obtained from Aladdin (Shanghai, China). The Alizarin red S staining (ARS), BCIP/NBT alkaline phosphatase colour development, alkaline phosphatase assay,

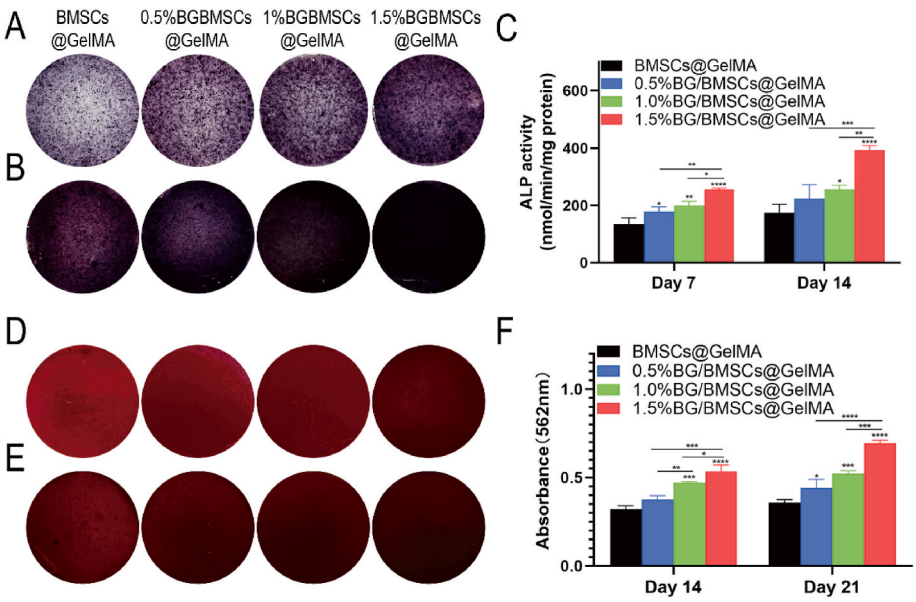

Fig. 3. Osteogenic differentiation of BMSCs in hydrogels. (A) ALP staining at day 7 (A) and 14 (B). (C) ALP activity assays at day 7 and 14. ARS at days 14 (D) and 21 (E). (F) Quantitative analysis of ARS.

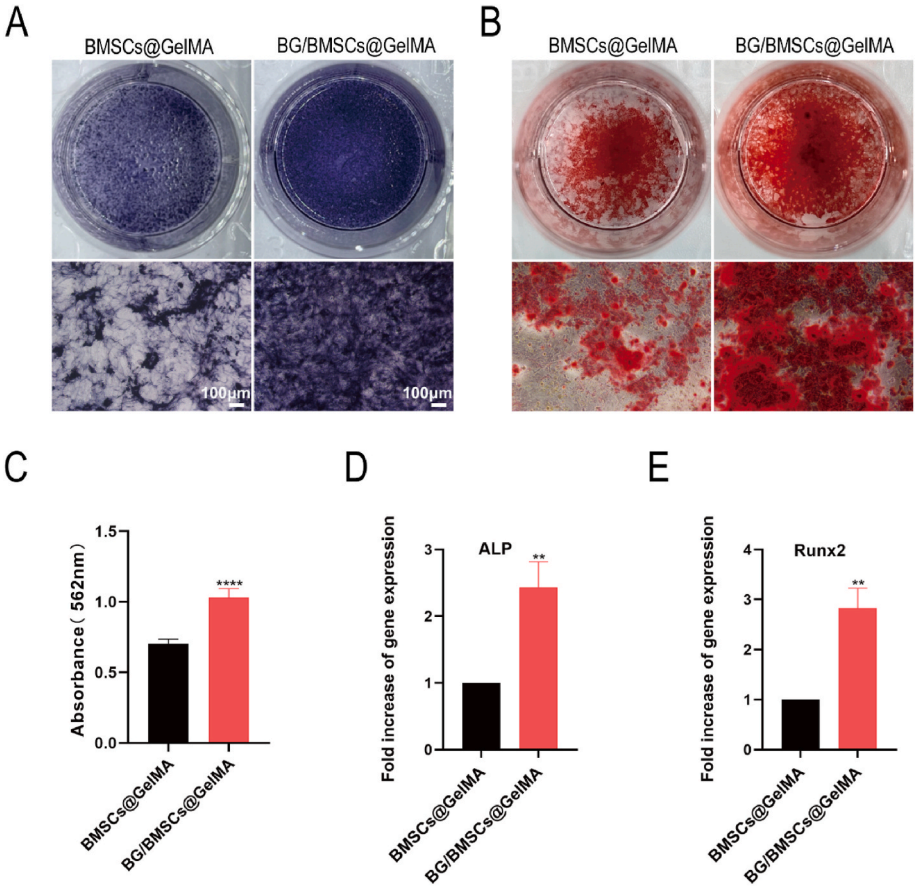

Fig. 4. (A) ALP staining of the MSCs co-cultured at day 7. (B) ARS staining of the MSCs co-cultured at day 14. (C) Quantitative analysis of ARS. Relative mRNA-expression levels of ALP (D) and RUNX2 (E) in BMSCs.

and BCA protein assay kits were obtained from Beyotime Biotechnology (Shanghai, China). Collagenase II was obtained from Enzyme Biotechnology (Shanghai, China).

2.2. Preparation of hydrogels

The composition of various bio-inks (Table 1). Briefly, GelMA were dissolved in deionized water in a beaker at 50 °C for 1 h. Subsequently,

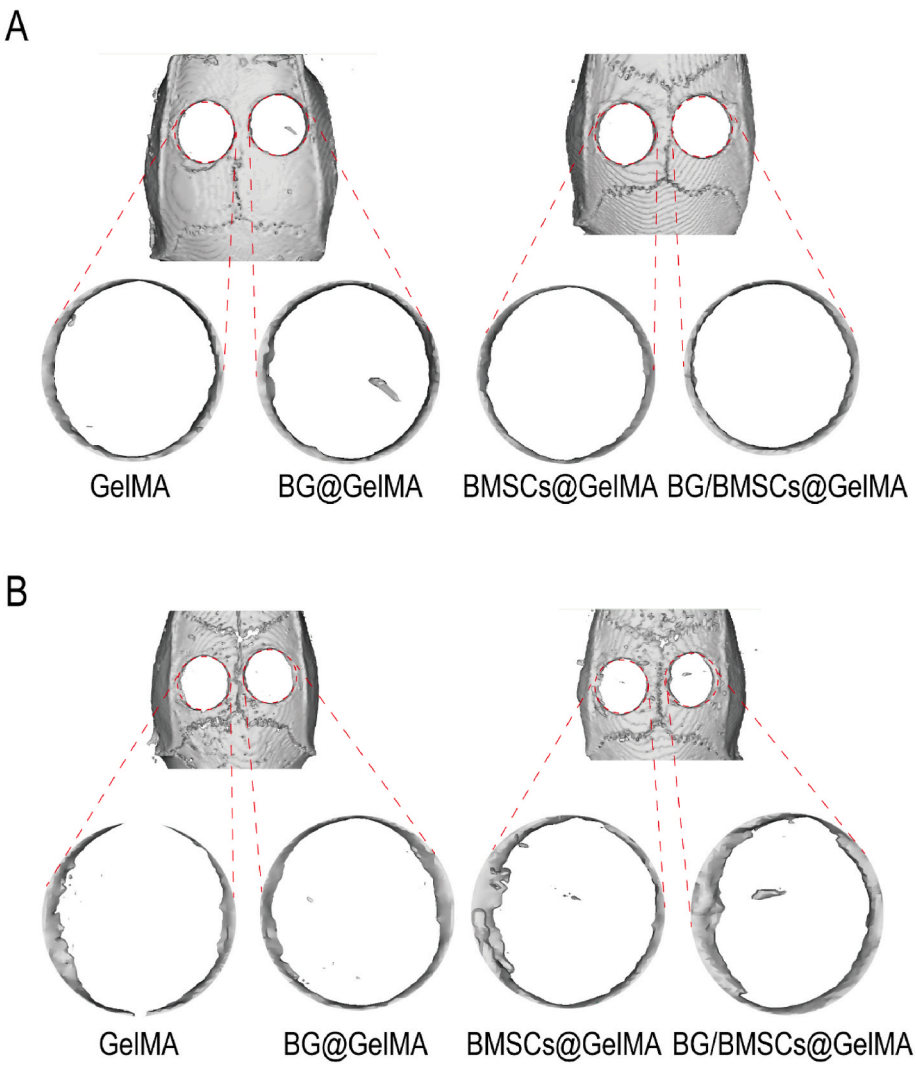

Fig. 5. Imaging evaluation 3 and 7 d after surgery in calvarial defect. Micro-CT images for 3 (A) and 7 d (B).

LAP and 45S5 BG were added to GelMA solution and continuously stirred in a 50 °C water bath for 2 h. The uniform bio-ink was obtained successfully.

2.3. Scanning electron microscopy (SEM)

The SEM (Zeiss) was used to observe the surface and interior of the hydrogel. The surface and internal surfaces of the lyophilised hydrogel samples were coated with gold-palladium for 3 min. SEM images were acquired at different magnifications.

2.4. Compressive mechanical properties

The compression mechanical properties of different hydrogels were tested using a electromechanical universal testing machine and a 5 N load cell. The slope of the strain range 0–10 % of the stress-strain curve was used to calculate the Young's modulus of the different hydrogels.

2.5. Swelling test

In order to detect swelling of different hydrogels, 5 % GelMA, 5 % GelMA/0.5 % BG, 5 % GelMA/1 % BG, 5 % GelMA/1.5 % BG, 5 % GelMA/2 % BG bio-inks were cured in a standard mould after exposure to UV light (405 nm) for 30 s. The hydrogels were lyophilised and weighed to determine their dry weight (W1). These hydrogels were then immersed in PBS at 40 °C. After soaking at different time points, the swelling weight (W2) was recorded. The swelling ratio was calculated as $Q = (W2–W1)/W1 \times 100\ \%$.

2.6. In vitro degradation test

The aforementioned methods were used in the swelling test to fabricate hydrogels to detected the degradations of 5 % GelMA, 5 % GelMA/0.5 % BG, 5 % GelMA/1 % BG, 5 % GelMA/1.5 % BG, and 5 % GelMA/2 % BG hydrogels. Different hydrogels were incubated at 37 °C using collagenase II. The hydrogels were removed at the appropriate time point. The sample was subsequently lyophilised and weighed (W1), and the dry weight at day 0 was recorded as W0. The degradation ratio was calculated as $DR = (W0–W1)/W0 \times 100\ \%$.

2.7. Cell culture

BMSCs were obtained from the femurs and tibia of Sprague–Dawley rats as reported previously [40]. Five healthy 1-week-old male rats were euthanised and immersed in 75 % alcohol for 5 min. The muscles and skin of both lower limbs were resected by aseptic surgery. The DMEM/F12 medium was sucked into the syringe to flush the bone marrow out of the bone cavity completely. Cells were cultured in DMEM/F12 complete culture medium at 37 °C under 5 % CO_2 conditions. The complete culture medium was replaced every 3 d. After the

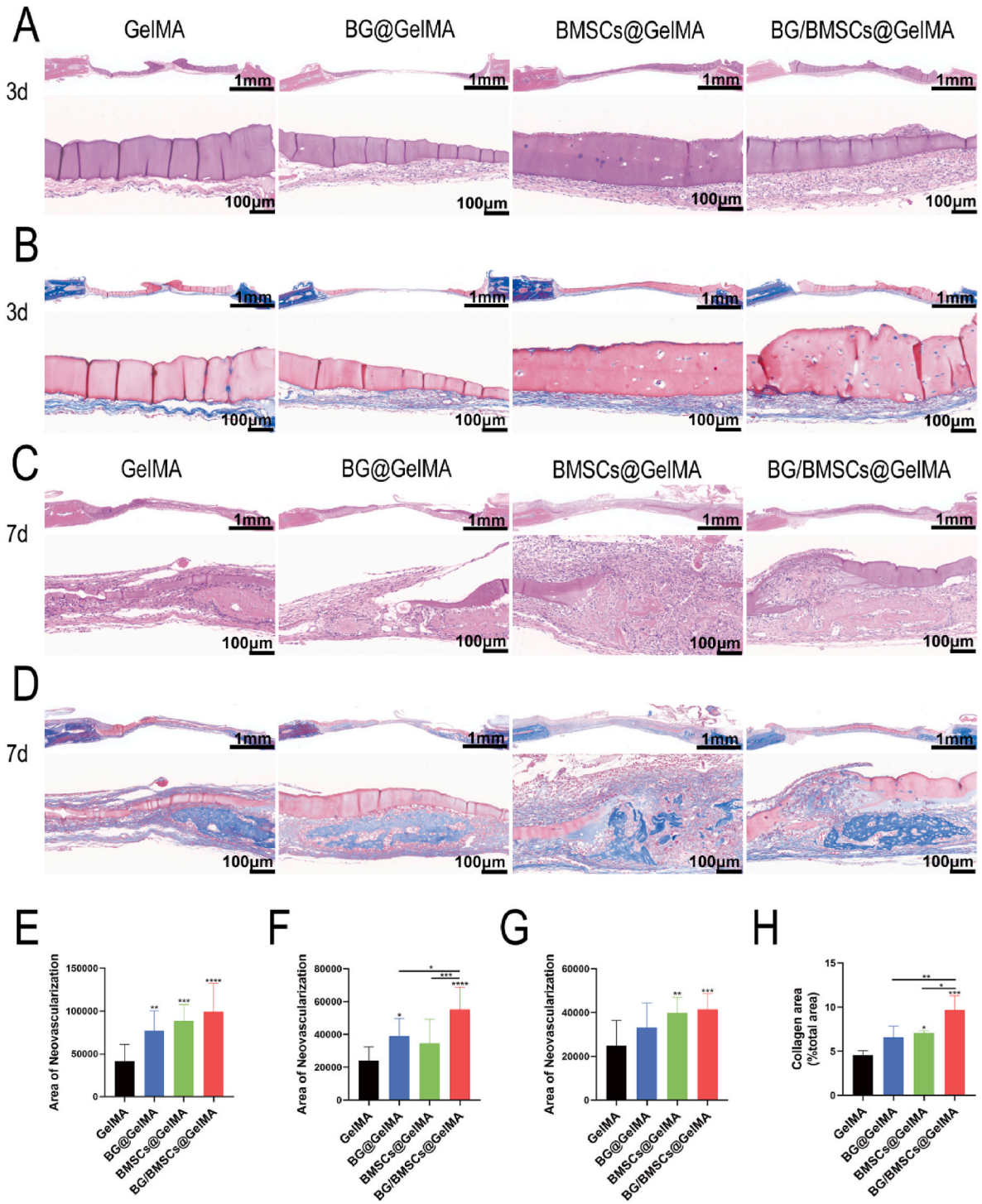

Fig. 6. Histological analysis at 3 and 7 d after implantation in rat calvarial defect. H&E and Masson's trichrome staining at 3 d (A, B) and 7 d (C, D). Area of neovascularization at day 7 (E), 28 (F), and 56 (G) after implantation, respectively. Area of collagen (% total area) at 7 d (H).

confluence reached 90 %, BMSCs were harvested and passaged. The experiment used third-generation BMSCs.

2.8. Preparation of BMSCs-laden hydrogels

BG, LAP, GelMA required for the experiment were accurately weighed. The GelMA and LAP were then mixed in DMEM/F12 medium, and filtered with a filter. The BG were exposed to UV for 48 h. To encapsulate BMSCs in the hydrogel, BMSCs (1×10^6 cells/mL) were transplanted into the GelMA pre-polymer (with or without bio-glass) followed by 30 s of UV irradiation for photo-crosslinking.

2.9. Cell viability analysis

The CCK-8 kit was used to detect cell proliferation. Briefly, cell-laden hydrogels were cultured for different times and 250 μL of CCK-8 solution was added to each well. The supernatant was used to measure optical density (OD) values after incubation at 37 °C for 2 h. The live/dead viability kit was used according to the manufacturer's instructions. Images were captured by fluorescence microscope.

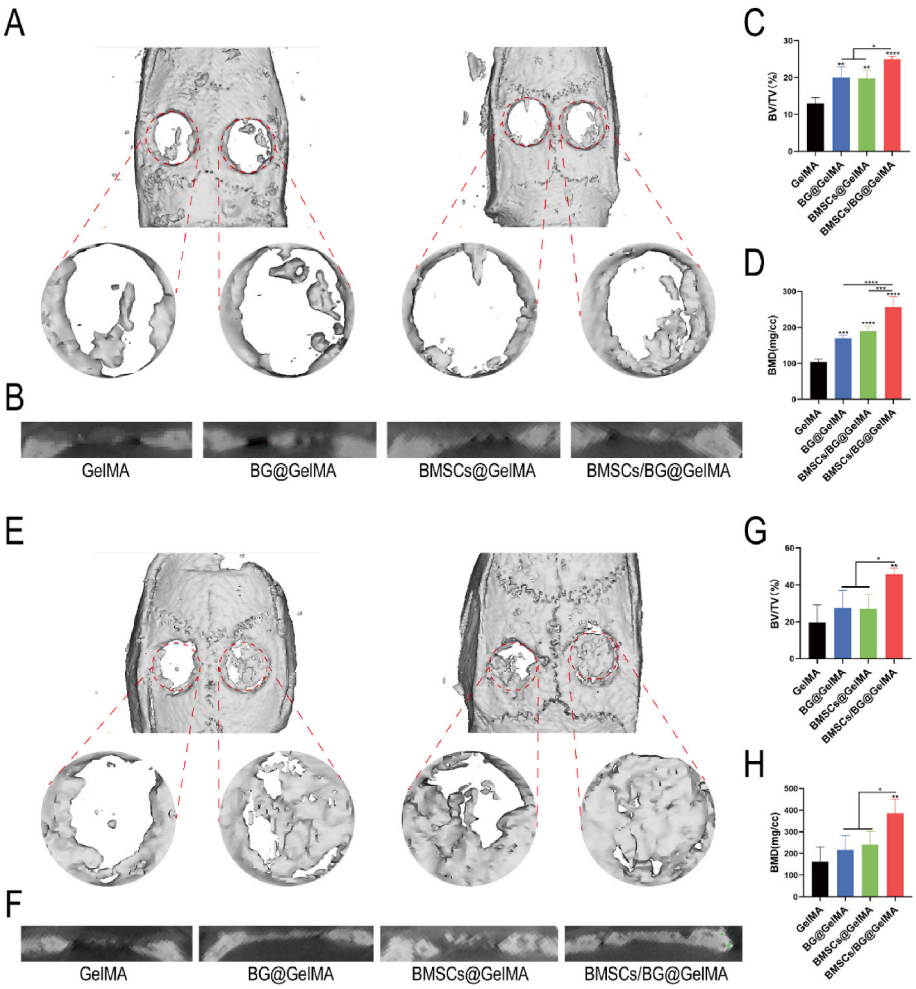

Fig. 7. Imaging evaluation 4 and 8 w after surgery in calvarial defect. Micro-CT images for 4 weeks (A) and sagittal images (B). BV/TV (C) and BMD (D) after 4 weeks. Micro-CT images for 8 weeks (E) and sagittal images (F). BV/TV (G) and BMD (H) after 8 weeks. Red dotted circle indicates the bone defect area. (For interpretation of the references to color in this figure legend, the reader is referred to the Web version of this article.)

2.10. Alkaline phosphatase (ALP) staining

The cell-laden hydrogels were cultured in osteogenic media for appropriate time. The hydrogels were washed three times and lysed the GelMA hydrogel with a GelMA lysis solution. When the cells were released from the hydrogel, the cells were lyzed using Western blotting and IP solutin. The cell solution was then centrifuged at 13,000 RPM for 10 min to collect the supernatant. ALP activity and protein concentration were detected by ALP assay kit and BCA protein assay kit, respectively. The cell-laden hydrogels were cultured in osteogenic media for different times. The hydrogels were washed with PBS, ALP staining was performed.

2.11. Alizarin red staining (ARS)

The cell-laden hydrogels were cultured in an osteogenic medium for different time. The hydrogels were washed with de-ionised water and fixed with paraformaldehyde. The cell-laden hydrogels were stained with the ARS. Camera and optical microscope were used to photograph the samples. In order to quantify calcium deposits inside the hydrogel, the nodules were immersed in 10 % cetylpyridine chlorinated solution and absorbance was determined at 562 nm.

2.12. Osteogenic gene expression

Briefly, BMSCs culture for 7 d, the total amount of RNA was extracted. Then, the RNA was reverse-transcribed to obtain complementary deoxyribonucleic acid (DNA) (cDNA). The mRNA expression of related genes was detected by qRT-PCR. The primer sequences are listed in Table S1.

2.13. In vivo calvarial defect model

All animal experiments were conducted in accordance with the Guidelines for the Care and Use of Experimental Animals of Nanchang University, and approved by the Animal Ethics Committee of Nanchang University. All the implanted BMSCs were allogeneic. The Sprague–Dawley rat cranial-defect was used to evaluate the bone regeneration of the hydrogels in each group in vivo. Thirty-two 12-week-old rats were given general anesthesia, and a sagittal incision was made directly above the skull. Two critical size defects with a diameter of 5 mm were drilled on both sides of the skull using a dental ring drill, and the hematoma was cleaned using sterile PBS, hydrogel was implanted, and wound was sutured. Implant four different hydrogels: (1) GelMA, (2) BG@GelMA, (3) BMSCs@GelMA, and (4) BG/BMSCs@GelMA (n = 4). The cell density of the BMSC-loaded hydrogels was 1×10^6 cells/ml. Four rats were randomly sacrificed from each group at 4 and 8 weeks after implantation, and samples were collected for further experiments.

2.14. Imaging analysis

Thirty-two rats in the GelMA, BG@GelMA, BMSCs@GelMA, and BG/

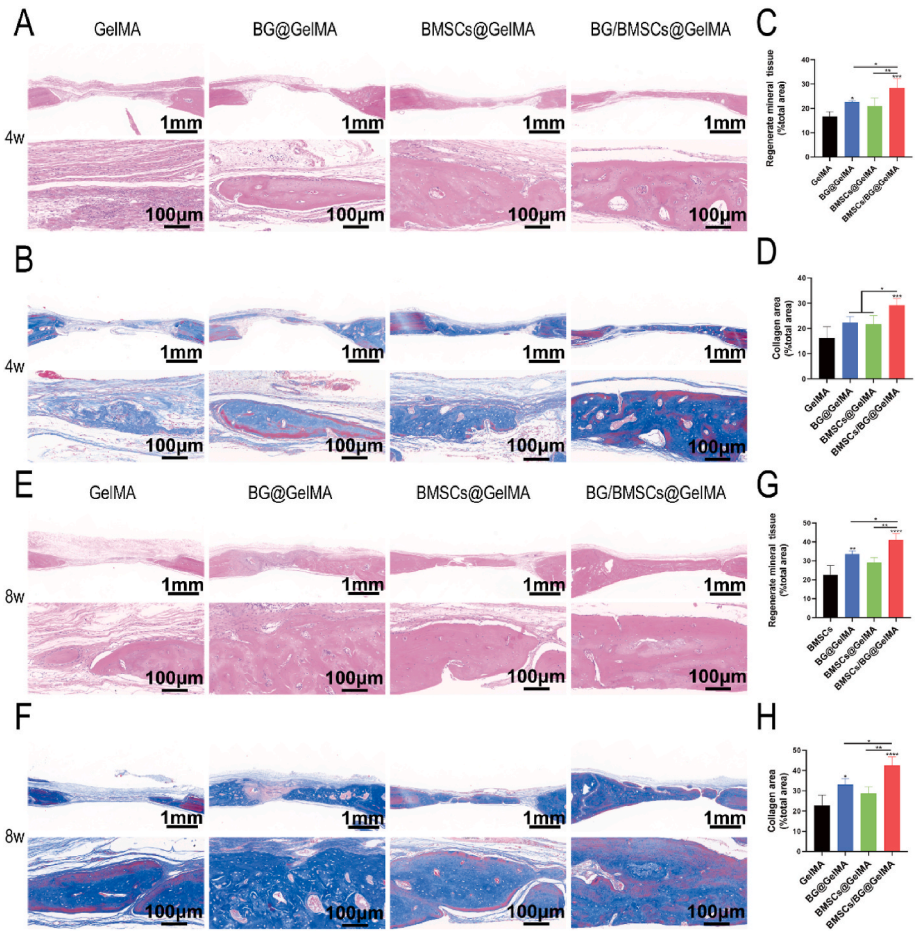

Fig. 8. Histological analysis at 4 and 8 w after implantation in rat calvarial defect. H&E and Masson's trichrome staining at 4 w (A, B) and 8 w (E, F). Percentage of new bone area in H&E at 4 w (C) and 8 w (G). Percentage of collagen area in Masson's trichrome at 4 w (D) and 8 w (H).

BMSCs@GelMA groups were respectively sacrificed at 3 d, 7 d, 4 weeks, and 8 weeks after surgery, and their skulls were removed. Samples were measured by a micro-CT scanning system. Briefly, the sample is scanned first in this study. The datas were reconstructed using three-dimensional (3D) surface rendering. Bone volume/tissue volume (BV/TV) as well as bone mineral content (BMD) were calculated using micro-CT analysis software after the defect area was identified.

2.15. Histological analysis

The skull specimens were fixed, decalcified, embedded, and then stained with H&E and Masson's trichrome. At days 3, 7, 28, and 56, particle analysis was performed using the ImageJ function of the same threshold range. The field of view was selected under an 80 × magnification, and three ROIs were randomly selected for each sample. The neovascularization area of the above ROI in the HE-stained tissue images were calculated using ImageJ software. The area of regenerated mineral tissue in H&E staining images was calculated using ImageJ to evaluate bone regeneration. The density of collagen in Masson's trichrome-stained images was calculated using ImageJ to evaluate bone regeneration.

2.16. Immunofluorescence staining

After routine dewaxing, the slices were boiled for 30 min. After cooling to 25 °C degrees, wash on a shaker three times for 5 min. The slices were incubated with 3 % bovine serum albumin and 0.1 % Triton X-100 for 20 min. The sections were then incubated with primary antibody at 4 °C overnight. After washed and incubated with fluorescent-labelled secondary antibodies , the sections were then immersed in 4 ′, 6-diamino-2-phenylindole (DAPI) and nucleated at 37 °C.

2.17. Statistical analyses

GraphPad Prism (version 9.0, manufacturer, location) was used for statistical analyses. The data were displayed as mean ± standard deviation. Data were compared with a one-way analysis of variance followed by Tukey's post-hoc test among groups. *P*-values <0.05 were defined as statistically significant.

3. Result and discussion

3.1. Characterisation of hydrogels

SEM was used to analyse the microporous structures of the GelMA and BG@GelMA hydrogels in situ. As shown in Fig. 1A, the GelMA hydrogel had interconnected and evenly distributed pores, which allowed the cells to attach inside the hydrogel and exchange substances with the outside environment. BG was evenly distributed in the GelMA hydrogel. The morphology of BMSCs in hydrogel was observed by SEM. Most cells were wrapped in the hydrogel, so they could not be observed directly. Only a rounded protrusion wrapped in the micro-filaments was visible (Fig. 1B (a1, b1)). Some studies have shown that the morphology of cells in a hydrogel can be outspread by extending the culture time. A few cells migrated from the inner parts to the surface of the hydrogel

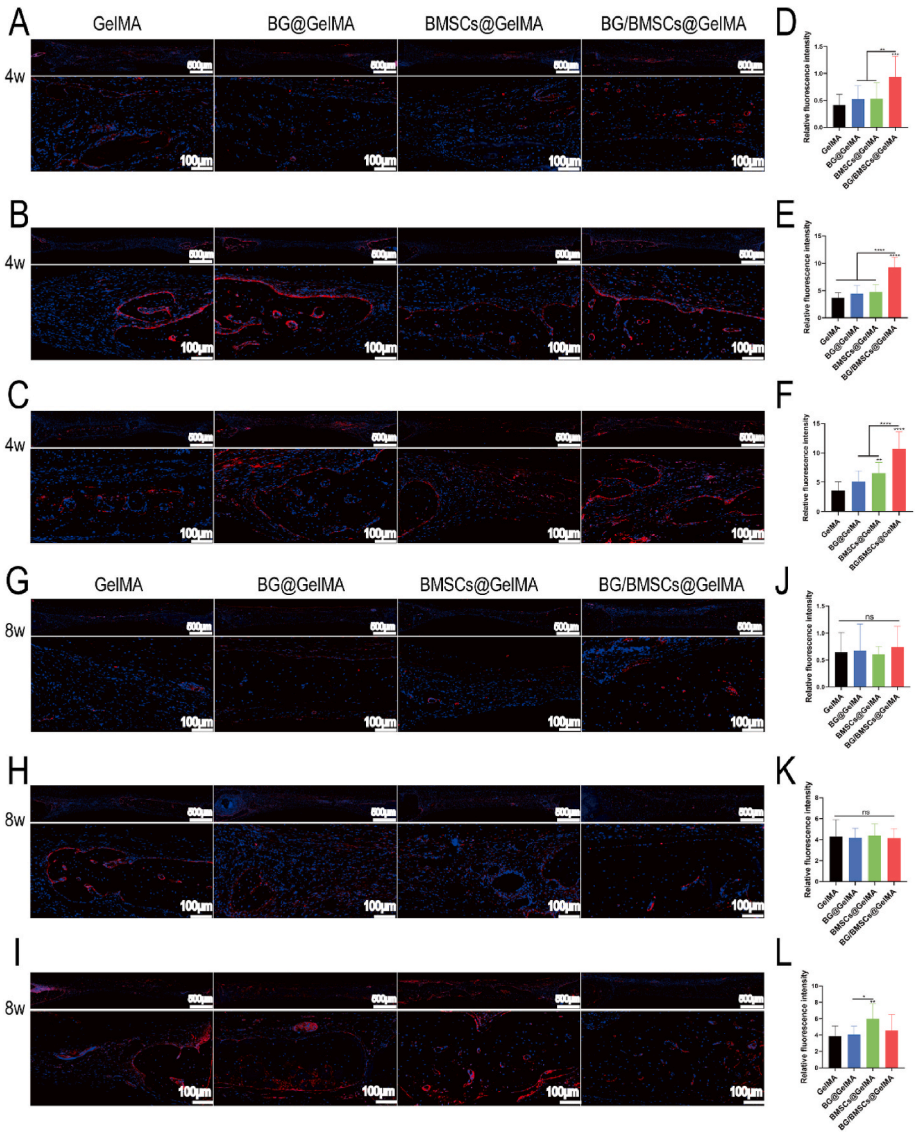

Fig. 9. Immunofluorescence staining in vivo. Immunostaining for CD31 (A), OCN (B) and OPN (C) at 4 weeks. Quantitative analysis of CD31 (D), OCN (E) and OPN (F) at 4 weeks. Immunostaining for CD31 (G), OCN (H) and OPN (I) at 8 weeks. Quantitative analysis of CD31 (J), OCN (K) and OPN (L) at 8 weeks.

(Fig. 1B (a2, b2)). As shown in Fig. 1B (a3, b3), the cells adhered to the hydrogel, and some of them were attracted by BG. The integrity of the scaffold is essential for cell culture [41,42]. In the collagenase degradation experiment, the GelMA hydrogels degraded completely in 2 h (Fig. 1C). However, the degradation rate decreases with the incorporation of BG into the hydrogel. In addition, the inclusion of BG reduced the swelling rate of the hydrogels, which may be due to its hydrophobicity (Fig. 1D). The data presented above show that BG incorporation delays the enzymatic degradation of the hydrogel and limits water penetration and volume changes after implantation to produce more stable constructs. The mechanical properties of the hydrogels were evaluated using uni-axial compression experiments. The stress at 50 % strain (Fig. 1E) and compressive modulus (Fig. 1F) of the GelMA hydrogels increased significantly at increasing BG concentrations. According to the results of the mechanical properties, addition of BG resulted in higher mechanical strength.

3.2. Cytocompatibility of hydrogels in vitro

Because BMSCs were crucial in the repair of bone defects, we examined the activity of the BMSCs encapsulated in the hydrogels. Studies have shown that lower concentrations of GelMA result in higher cell viability than high concentrations of GelMA. Therefore, 5 % GelMA hydrogel was used to encapsulate the cells in this study. The results of the live/dead assays showed that more than 80 % of the cells were viable from d 1 to d 7 in all groups, except the 2.0 % BG/BMSCs@GelMA group (Fig. 2A). In addition, no significant differences in the OD values were observed in any of the groups on day 1, 3, and 7, except for the 2.0 % BG/BMSCs@GelMA group (Fig. 2B and C). These results demonstrate that the BMSCs@GelMA, 0.5 % BG/BMSCs@GelMA, 1.0 % BG/BMSCs@GelMA, and 1.5 % BG/BMSCs@GelMA hydrogels exhibited good biocompatibility. These hydrogels were used in subsequent experiments.

3.3. Osteogenic differentiation of BMSCs

The ideal biological scaffold should be able to promote the osteogenic differentiation of BMSCs. However, GelMA hydrogel only provides a stable 3D micro-environment for cells, and its insufficient osteoinduction ability limits its applications. Study have shown that BG promotes osteogenic differentiation of bone marrow mesenchymal stem cells through BMP/Smad signaling pathway [43]. Cui et al.

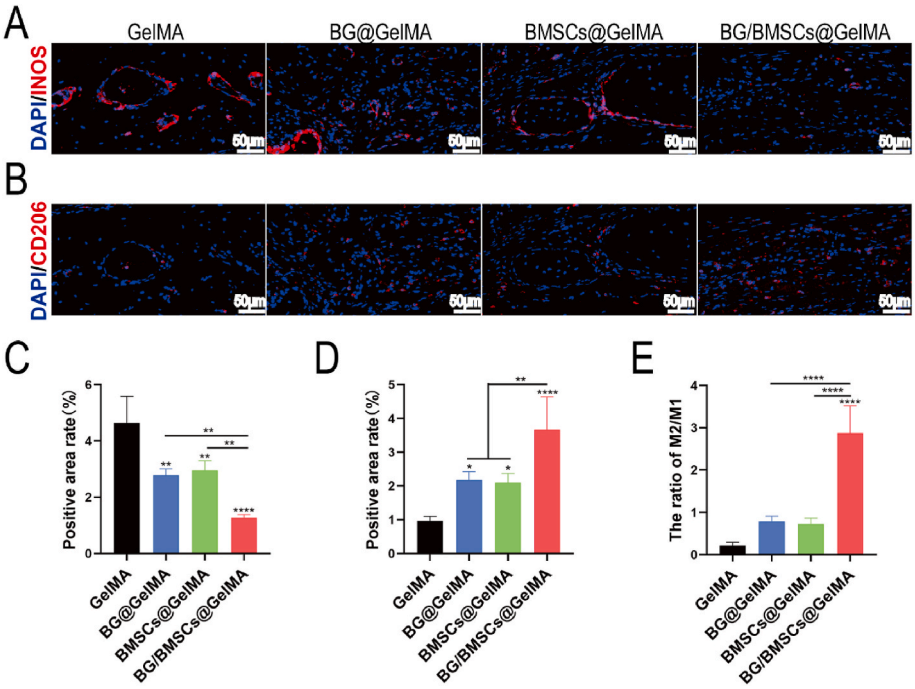

Fig. 10. Immunofluorescence staining analysis. Immunofluorescence staining images of iNOS (A) and CD206 (B) in rats following different treatments, and orresponding expression analysis of iNOS (C), and CD206 (D). Ratio of expression of CD206 (M2) to iNOS (M1) (E).

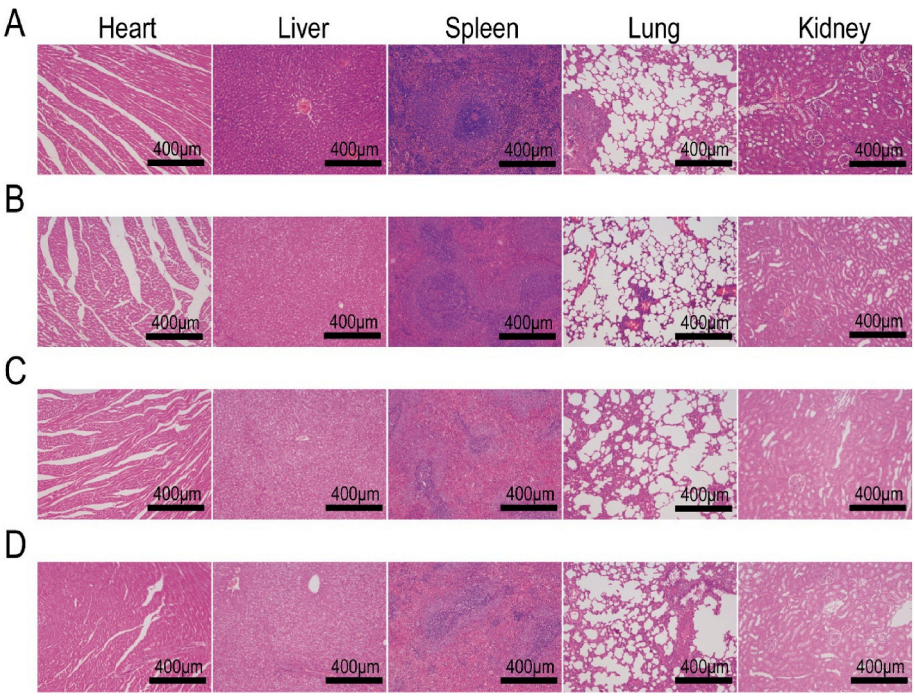

Fig. 11. Schematic illustration of in vivo evaluation. H&E Staining of organs implanted with GelMA-BG@GelMA (A) and BMSCs@GelMA-BG/BMSCs@GelMA(B) for 4 weeks, and GelMA-BG@GelMA(C) and BMSCs@GelMA-BG/BMSCs@GelMA(D) for 8 weeks (bar = 400 μm).

demonstrated that bone cement containing BG stimulates bone regeneration of femoral condylar defect in rabbits by activating Wnt/β-catenin signaling pathway [44]. Therefore, the incorporation of BG is essential for the osteogenic properties of hydrogels. ALP and ARS were used to detect osteogenic differentiation of BMSCs [45]. As shown in Fig. 3A–C, ALP expression was higher in the 0.5%BG/BMSCs@GelMA, 1.0%BG/BMSCs@GelMA, and 1.5%BG/BMSCs@GelMA compared with the GelMA group; moreover, compared with the 0.5% BG/BMSCs@GelMA and 1.0%BG/BMSCs@GelMA, the 1.5% BG/BMSCs@GelMA group exhibited enhanced ALP staining and increased ALP activity. Mineralised nodules are markers of osteoblast differentiation and maturation. ARS was performed to detect the effects of the hydrogels on the mineralisation of BMSCs (Fig. 3D–F). The number of bone mineralisation nodules increased significantly in the BG/BMSCs@GelMA group. Bone mineralisation in the 1.5% BG/BMSCs@GelMA group significantly increased among the three

groups. Quantitative analyses further indicated that 1.5% BG/BMSCs@GelMA promoted the formation of mineralised modules. Based on above results, we believed that the 1.5%BG/BMSCs@GelMA hydrogel promotes osteogenic differentiation of BMSCs, and the 1.5% BG/BMSCs@GelMA hydrogel was used in the in vivo study.

The material was co-cultured with BMSCs to verify its effect on osteogenic differentiation of BMSCs. The qRT-PCR was used to evaluate the effect of hydrogels on marker genes for the osteogenic differentiation of BMSCs. The data indicated that the expression levels of ALP (Fig. 4D) and Runx2 (Fig. 4E), bio-marker genes of osteoblast differentiation, were significantly higher in the BG/BMSCs@GelMA group than BMSCs@GelMA group [46]. In addition, the ALP and ARS staining results indicated that the degree of ALP and ARS staining was more obvious in the BG/BMSCs@GelMA group (Fig. 4A–C).

3.4. In vivo bone regeneration of hydrogels

BG/BMSCs@GelMA hydrogels have been shown to have desirable cellular biocompatibility and excellent osteo-induction effects in vitro. In this study, a rat cranial defect model was used to evaluate further the osteogenic effects of BG/BMSCs@GelMA. Two 5 mm diameter critical-sized bone defects were drilled on both sides of the skulls of the rats and implanted with different hydrogels. Subsequently, in situ, optical crosslinking was performed using UV light (405 nm).

The hematoma begins to dissipate on the third day after the fracture, with the local release of cytokines to recruit stem cells. At seven days after fracture, local cartilage callus and unmineralized cartilage tissue formed. Therefore, we chose to examine the bone defect area to explore the process of early osteogenesis at day three and seven after implantation. Micro-CT was performed to observe early osteogenesis. Three days after implantation, there was no new bone tissue in any group (Fig. 5A). Seven days after implantation, there was a small amount of new bone tissue between the material and host bone (Fig. 5B). Stem cells in the initial inflammatory phase do not proliferate or differentiate.

After the implantation of hydrogels, the ideal hydrogel structure is gradually degraded and absorbed, while the cells in the scaffold proliferate and secrete the ECM into the body to achieve bone regeneration. Three days after implantation, the hydrogel scaffold was relatively complete, without fracture or collapse, and played a supporting role. A small number of fibroblasts and a limited degree of angiogenesis were observed at the bottom of the hydrogel, and no new bone tissue was observed in any group (Fig. 6A and B). Seven days after implantation, a large number of vessels and new collagen were observed in each group, whereas the BG/BMSCs@GelMA group exhibited the best new bone and blood vessel production outcomes (Fig. 6C–E). Interestingly, hydrogels in the BG@GelMA, BMSCs@GelMA, and BG/BMSCs@GelMA groups degraded faster compared with the GelMA group. Mass cells were observed around the hydrogels, and some cells entered the hydrogels, thus indicating that the hydrogels promoted cell migration. Wang et al. [47] showed that BG promotes BMSCs migration through ionic dissociation products. Furthermore, studies have shown that MSCs stimulate the migration of MSCs and endothelial cells via a paracrine mechanism [48]. The aforementioned studies showed that the BG@GelMA, BMSCs@GelMA, and BG/BMSCs@GelMA groups had higher cell infiltration and angiogenesis than the GelMA group.

The hydrogel completely degraded 4 weeks after surgery. At week 4 after surgery, new bone tissue was formed in all groups, with the BG/BMSCs@GelMA group yielding the best new bone production (Fig. 7A–D). The difference in new bone formation was more pronounced, with the new bone volume of the BG/BMSCs@GelMA group being significantly higher than those in other groups at 8 weeks after surgery (Fig. 7E and F). Quantitative analyses of BV/TV and BMD further demonstrated the effect of BG/BMSCs@GelMA on bone regeneration (Fig. 7G and H).

Subsequently, H&E staining showed that at 4 and 8 weeks after implantation, there were new bones in all groups. Four weeks after surgery (Fig. 8A–D), the BG/BMSCs@GelMA group had a higher content of new bone, followed by the BG@GelMA and BMSCs@GelMA groups. However, there was only a little of new bone in the GelMA group, which was mainly fibrous tissue. New bone tissues were mainly distributed at the interface between the hydrogels and host tissue. Eight weeks after surgery (Fig. 8E–H), especially in the BG/BMSCs@GelMA group, a large amount of new bone tissue was formed in the centre of the defect area, and these new bones occupied almost the entire bone defect area. Masson's trichrome staining confirmed the presence of new bone formation in all groups, and the BG/BMSCs@GelMA had a better bone composition effect than the other groups.

Bone is connective tissue rich in blood vessels, and early angiogenesis is essential for bone regeneration [49–52]. BG promotes vascular regeneration and is extensively used in wound repair and bone regeneration [35,53]. At four weeks, the BG@GelMA had more new blood vessels than GelMA group (Fig. 6F). Studies [54,55] have shown that BMSCs co-culture with human umbilical vein endothelial cells promotes the vascularization of bone tissue, which may be caused by the secretion of vascular endothelial and other growth factors by BMSCs. The data of H&E staining indicated that the BMSCs@GelMA group had a higher number of new vessels than the GelMA group at 4 weeks after implantation. In order to further detect the angiogenesis in the defect area, immunofluorescence staining was performed. The result of immunostaining showed that the expression of CD31 was significantly higher in the BG/BMSCs@GelMA group than the other groups at week 4 after surgery (Fig. 9A and D). This proved that the BG/BMSCs@GelMA group had the highest number of blood vessels among the four groups which is consistent with above results. Interestingly, there was no significant difference in fluorescence intensity among four groups at 8 weeks (Fig. 9G and J).

Our results showed that the immunofluorescence intensity of the BG/BMSCs@GelMA group was the highest. The quantitative analysis showed that the expression of the osteoblast markers OCN (Fig. 9B and E) and OPN (Fig. 9C and F) was significantly higher in the BG/BMSCs@GelMA group than the other groups at week 4 after surgery [56–58]. This demonstrates the positive effect of BG/BMSCs@GelMA on osteogenesis. Interestingly, the expression levels of OCN (Fig. 9H and K) and OPN (Fig. 9I, L) decreased at 8 weeks after implantation in the BG/BMSCs@GelMA group compared with 4 weeks. We believe that these results were due to the formation of a large number of new bone tissues in the BG/BMSCs@GelMA group at 8 weeks, in which the osteoblasts were wrapped by bone tissues and matured into bone cells.

Growing studies [33,59] have proved that the behavior of host-cells and the occurrence and development of diseases were affected by the local microenvironment. Persistent inflammatory states, such as persistent M1 macrophage activation, may affect the immune-regulated osteogenesis process and delay bone regeneration. Whether biomaterials regulate the host immune response to provide a suitable immune microenvironment for bone tissue regeneration are very vital for bone regeneration. Macrophages play an important role in regulating multiple stages of bone tissue repair. Macrophages can transform into different phenotypes in different microenvironments. As shown in Fig. 10, at 4 weeks after surgery, Immunofluorescence staining showed that CD206 fluorescence staining intensity increased after adding BG. This indicates that the addition of BG promotes the polarization of macrophages towards M2 type, thus promoting bone tissue regeneration. iNOS fluorescence intensity was significantly reduced, while CD206 fluorescence intensity was significantly increased after BG/BMSCs@GelMA hydrogel treatment compared with other groups. Quantitative analysis results showed that BG/BMSCs@GelMA hydrogel had the highest M2/M1 ratio. The above results indicated that BG/BMSCs@GelMA hydrogel efficiently enhances the transition of macrophages from the M1 to the M2 phenotype.

In order to detect the toxicity of hydrogels in vivo, major organs of rats were histologically stained, H&E staining revealed that the hearts, livers, spleens, lungs, and kidneys of SD rats treated with bioactive

hydrogel scaffolds did not exhibit significant inflammation or damage (Fig. 11A–D). Overall, these results demonstrated that the hydrogel scaffolds in each group had good biocompatibility.

This study is associated with some limitations. Some studies have proved that scaffold-encapsulated cells have positive effect on bone tissue regeneration and may play a therapeutic role by differentiating into specific cells or paracrine. In this study, we prepared a hydrogel loaded with BMSCs to promote bone regeneration in rat cranial defects. However, this study did not explore the proliferation of BMSCs within the hydrogel in vivo, which is a limitation. Second, We have studied the effects of BG on BMSCs differentiation but did not detect the effects of BG on BMSCs paracrine signalling. Our future studies will focus on exploring the paracrine effects of BG on BMSCs and observing the proliferation of BMSCs in the hydrogel implanted in vivo.

4. Conclusions

Recently, research based on stem cell therapy has been extensively used to repair bone defects. In this study, we successfully designed an in-situ photopolymerised, and cost-effective BG/BMSCs@GelMA hydrogel. In vitro experiments indicated that addition of BG enhanced osteoinduction of the hydrogels. The composite hydrogel scaffold further promoted angiogenesis and mineralisation of the bone defect areas, which is crucial for the bone regeneration. In addition, this composite bioactive hydrogel scaffold, with excellent biocompatibility and osteogenic activity, is a promising material for bone regeneration.

Statement of significance

There are many therapeutic methods for bone-defect repair, but these are limited by the insufficient number of transplanted bones, rejection reactions, and limited osteogenic capabilities. In this study, BG/BMSCs@GelMA with osteogenic and angiogenic properties was developed for bone-defect repair. 1) BG/BMSCs@GelMA exhibited excellent cytocompatibility. 2) BG promoted the osteogenic differentiation of BMSCs in the BG/BMSCs@GelMA hydrogel and co-cultured BMSCs. 3) In the rat cranial-defect model, BG/BMSCs@GelMA recruited cells, promoted vascular regeneration in the early osteogenic stage, and showed significant bone regeneration performance 8 weeks after implantation. 4) BG/BMSCs@GelMA demonstrated immunomodulatory properties and promoted macrophage polarization towards M2 type. In conclusion, BG/BMSCs@GelMA can be used as a promising graft for the treatment of bone defects.

Declaration of competing interest

The authors declare that they have no known competing financial interests or personal relationships that could have appeared to influence the work reported in this paper.

Data availability

Data will be made available on request.

Acknowledge

This work was financially supported by the National Natural Science Foundation of China (No. 82060203 to L.S. and No. 31960207 to F.A.), the Interdisciplinary Innovation Fund of Natural Science, Nanchang University (No.9166-27060003-ZD04 to L.S.) and the Science Fund for Distinguished Young Scholars of Jiangxi Province (No. 20224ACB214005 to F.A.)

Appendix A. Supplementary data

Supplementary data to this article can be found online at https://doi.org/10.1016/j.mtbio.2023.100882.

References

[1] Y. Sun, X. Liu, Y. Zhu, Y. Han, J. Shen, B. Bao, T. Gao, J. Lin, T. Huang, J. Xu, Y. Chai, X. Zheng, Tunable and controlled release of cobalt ions from metal-organic framework hydrogel nanocomposites enhances bone regeneration, ACS Appl. Mater. Inter. 13 (2021) 16.
[2] Z. Shi, Q. Zhong, Y. Chen, J. Gao, X. Pan, Q. Lian, R. Chen, P. Wang, J. Wang, Z. Shi, H. Cheng, Nanohydroxyapatite, nanosilicate-reinforced injectable, and biomimetic gelatin-methacryloyl hydrogel for bone tissue engineering, Int. J. Nanomed. 16 (2021) 5603–5619.
[3] S. Ravindran, M. Kotecha, C.C. Huang, A. Ye, P. Pothirajan, Z. Yin, R. Magin, A. George, Biological and MRI Characterization of Biomimetic ECM Scaffolds for Cartilage Tissue Regeneration, 2015.
[4] M. Yuan, K. Liu, T. Jiang, S. Li, J. Chen, Z. Wu, W. Li, R. Tan, W. Wei, X. Yang, H. Dai, Z. Chen, GelMA/PEGDA microneedles patch loaded with HUVECs-derived exosomes and Tazarotene promote diabetic wound healing, J. Nanobiotechnol. 20 (2022) 147.
[5] K. Yue, S.G. Trujillo-de, M.M. Alvarez, A. Tamayol, N. Annabi, A. Khademhosseini, Synthesis, properties, and biomedical applications of gelatin methacryloyl (GelMA) hydrogels, Biomaterials 73 (2015) 254–271.
[6] S. Li, J. Sun, J. Yang, Y. Yang, H. Ding, B. Yu, K. Ma, M. Chen, Gelatin methacryloyl (GelMA) loaded with concentrated hypoxic pretreated adipose-derived mesenchymal stem cells(ADSCs) conditioned medium promotes wound healing and vascular regeneration in aged skin, Biomater. Res. 27 (2023) 11.
[7] B. Lv, L. Lu, L. Hu, P. Cheng, Y. Hu, X. Xie, G. Dai, B. Mi, X. Liu, G. Liu, Recent advances in GelMA hydrogel transplantation for musculoskeletal disorders and related disease treatment, Theranostics 13 (2023) 2015–2039.
[8] H. Wu, Y. Shang, W. Sun, X. Ouyang, W. Zhou, J. Lu, S. Yang, W. Wei, X. Yao, X. Wang, X. Zhang, Y. Chen, Q. He, Z. Yang, H. Ouyang, Seamless and early gap healing of osteochondral defects by autologous mosaicplasty combined with bioactive supramolecular nanofiber-enabled gelatin methacryloyl (BSN-GelMA) hydrogel, Bioact. Mater. 19 (2023) 88–102.
[9] N. Hu, Z. Cai, X. Jiang, C. Wang, T. Tang, T. Xu, H. Chen, X. Li, X. Du, W. Cui, Hypoxia-pretreated ADSC-derived exosome-embedded hydrogels promote angiogenesis and accelerate diabetic wound healing, Acta Biomater. 157 (2023) 175–186.
[10] Q. Zhang, T. Yang, R. Zhang, X. Liang, G. Wang, Y. Tian, L. Xie, W. Tian, Platelet lysate functionalized gelatin methacrylate microspheres for improving angiogenesis in endodontic regeneration, Acta Biomater. 136 (2021) 441–455.
[11] J. Liu, B. Zhang, L. Li, J. Yin, J. Fu, Additive-lathe 3D bioprinting of bilayered nerve conduits incorporated with supportive cells, Bioact. Mater. 6 (2021) 219–229.
[12] G. Jiang, S. Li, K. Yu, B. He, J. Hong, T. Xu, J. Meng, C. Ye, Y. Chen, Z. Shi, G. Feng, W. Chen, S. Yan, Y. He, R. Yan, A 3D-printed PRP-GelMA hydrogel promotes osteochondral regeneration through M2 macrophage polarization in a rabbit model, Acta Biomater. 128 (2021) 150–162.
[13] Z. Liu, Y. Li, J. Yang, J. Huang, C. Luo, J. Zhang, W. Yan, Y. Ao, Bone morphogenetic protein 9 enhances osteogenic and angiogenic responses of human amniotic mesenchymal stem cells cocultured with umbilical vein endothelial cells through the PI3K/AKT/m-TOR signaling pathway, Aging (Albany NY) 13 (2021) 24829–24849.
[14] D. Chen, P. Chang, P. Ding, S. Liu, Q. Rao, O.V. Okoro, L. Wang, L. Fan, A. Shavandi, L. Nie, MSCs-laden silk Fibroin/GelMA hydrogels with incorporation of platelet-rich plasma for chondrogenic construct, Heliyon 9 (2023), e14349.
[15] X. Yu, X. Wang, D. Li, R. Sheng, Y. Qian, R. Zhu, X. Wang, K. Lin, Mechanically reinforced injectable bioactive nanocomposite hydrogels for in-situ bone regeneration, Chem. Eng. J. 433 (2022), 132799.
[16] Y. Huan, D. Zhou, X. Wu, X. He, H. Chen, S. Li, B. Jia, Y. Dou, X. Fei, S. Wu, J. Wei, Z. Fei, T. Xu, F. Fei, 3D bioprinted autologous bone particle scaffolds for cranioplasty promote bone regeneration with both implanted and native BMSCs, Biofabrication 15 (2023), 25016.
[17] X. Sun, Z. Ma, X. Zhao, W. Jin, C. Zhang, J. Ma, L. Qiang, W. Wang, Q. Deng, H. Yang, J. Zhao, Q. Liang, X. Zhou, T. Li, J. Wang, Three-dimensional bioprinting of multicell-laden scaffolds containing bone morphogenic protein-4 for promoting M2 macrophage polarization and accelerating bone defect repair in diabetes mellitus, Bioact. Mater. 6 (2021) 757–769.
[18] S. Chai, J. Huang, A. Mahmut, B. Wang, Y. Yao, X. Zhang, Z. Zhuang, C. Xie, Z. Xu, Q. Jiang, Injectable photo-crosslinked bioactive BMSCs-BMP2-GelMA scaffolds for bone defect repair, Front. Bioeng. Biotech. 10 (2022), 875363.
[19] Z. Li, S. Li, J. Yang, Y. Ha, Q. Zhang, X. Zhou, C. He, 3D bioprinted gelatin/gellan gum-based scaffold with double-crosslinking network for vascularized bone regeneration, Carbohyd. Polym. 290 (2022), 119469.
[20] R.D. Dickerman, A.S. Reynolds, B.C. Morgan, J. Tompkins, J. Cattorini, M. Bennett, rh-BMP-2 can be used safely in the cervical spine: dose and containment are the keys, Spine J. 7 (2007) 508–509.
[21] M.M. Azevedo, O. Tsigkou, R. Nair, J.R. Jones, G. Jell, M.M. Stevens, Hypoxia inducible factor-stabilizing bioactive glasses for directing mesenchymal stem cell behavior, Tissue Eng. 21 (2015) 382–389.
[22] L.L. Hench, J.M. Polak, Third-generation biomedical materials, Science 295 (2002) 1014–1017.
[23] X. Zhou, J. Chen, H. Sun, F. Wang, Y. Wang, Z. Zhang, W. Teng, Y. Ye, D. Huang, W. Zhang, X. Mo, A. Liu, P. Lin, Y. Wu, H. Tao, X. Yu, Z. Ye, Spatiotemporal regulation of angiogenesis/osteogenesis emulating natural bone healing cascade for vascularized bone formation, J. Nanobiotechnol. 19 (2021) 420.

[24] D. Barati, S.R.P. Shariati, S. Moeinzadeh, J.M. Melero-Martin, A. Khademhosseini, E. Jabbari, Spatiotemporal release of BMP-2 and VEGF enhances osteogenic and vasculogenic differentiation of human mesenchymal stem cells and endothelial colony-forming cells co-encapsulated in a patterned hydrogel, J. Control Release 223 (2016) 126–136.
[25] Z. Wu, D. He, H. Li, Bioglass enhances the production of exosomes and improves their capability of promoting vascularization, Bioact. Mater. 6 (2021) 13.
[26] Y. Zhu, Z. Ma, L. Kong, Y. He, H.F. Chan, H. Li, Modulation of macrophages by bioactive glass/sodium alginate hydrogel is crucial in skin regeneration enhancement, Biomaterials 256 (2020) 14.
[27] M.N. Rahaman, D.E. Day, B.S. Bal, Q. Fu, S.B. Jung, L.F. Bonewald, A.P. Tomsia, Bioactive glass in tissue engineering, Acta Biomater. 7 (2011) 2355–2373.
[28] Z. Wu, J. Bai, G. Ge, T. Wang, S. Feng, Q. Ma, X. Liang, W. Li, W. Zhang, Y. Xu, K. Guo, W. Cui, G. Zha, D. Geng, Regulating macrophage polarization in high glucose microenvironment using lithium-modified bioglass-hydrogel for diabetic bone regeneration, Adv. Healthc. Mater. 11 (2022).
[29] Y.G. Yoshida, S. Yan, H. Xu, J. Yang, Novel metal nanomaterials to promote angiogenesis in tissue regeneration, Eng Regen 4 (2023) 265–276.
[30] Y. Li, X. Zhang, D. He, Z. Ma, K. Xue, H. Li, 45S5 Bioglass (R) works synergistically with siRNA to downregulate the expression of matrix metalloproteinase-9 in diabetic wounds, Acta Biomater. 145 (2022) 18.
[31] H. Wei, J. Cui, K. Lin, J. Xie, X. Wang, Recent advances in smart stimuli-responsive biomaterials for bone therapeutics and regeneration, Bone Res. 10 (2022) 17.
[32] W. Li, F. Dai, S. Zhang, F. Xu, Z. Xu, S. Liao, L. Zeng, L. Song, F. Ai, Pore size of 3D-printed polycaprolactone/polyethylene glycol/hydroxyapatite scaffolds affects bone regeneration by modulating macrophage polarization and the foreign body response, ACS Appl. Mater. Inter. 14 (2022) 20693–20707.
[33] Y. Wang, J. Wang, R. Gao, X. Liu, Z. Feng, C. Zhang, P. Huang, A. Dong, D. Kong, W. Wang, Biomimetic glycopeptide hydrogel coated PCL/nHA scaffold for enhanced cranial bone regeneration via macrophage M2 polarization-induced osteo-immunomodulation, Biomaterials 285 (2022), 121538.
[34] X. Chen, Z. Wan, L. Yang, S. Song, Z. Fu, K. Tang, L. Chen, Y. Song, Exosomes derived from reparative M2-like macrophages prevent bone loss in murine periodontitis models via IL-10 mRNA, J. Nanobiotechnol. 20 (2022) 110.
[35] K. Zheng, W. Niu, B. Lei, A.R. Boccaccini, Immunomodulatory bioactive glasses for tissue regeneration, Acta Biomater. 133 (2021) 168–186.
[36] T. Li, M. Peng, Z. Yang, X. Zhou, Y. Deng, C. Jiang, M. Xiao, J. Wang, 3D-printed IFN-gamma-loading calcium silicate-beta-tricalcium phosphate scaffold sequentially activates M1 and M2 polarization of macrophages to promote vascularization of tissue engineering bone, Acta Biomater. 71 (2018) 96–107.
[37] X. Lu, K. Li, Y. Xie, S. Qi, Q. Shen, J. Yu, L. Huang, X. Zheng, Improved osteogenesis of boron incorporated calcium silicate coatings via immunomodulatory effects, J. Biomed. Mater. Res. A 107 (2019) 12–24.
[38] Y. Zhu, Z. Ma, L. Kong, Y. He, H.F. Chan, H. Li, Modulation of macrophages by bioactive glass/sodium alginate hydrogel is crucial in skin regeneration enhancement, Biomaterials 256 (2020), 120216.
[39] X. Dong, J. Chang, H. Li, Bioglass promotes wound healing through modulating the paracrine effects between macrophages and repairing cells, J. Mater. Chem. B 5 (2017) 5240–5250.
[40] J. Gu, Q. Zhang, M. Geng, W. Wang, J. Yang, A.U.R. Khan, H. Du, Z. Sha, X. Zhou, C. He, Construction of nanofibrous scaffolds with interconnected perfusable microchannel networks for engineering of vascularized bone tissue, Bioact. Mater. 6 (2021) 3254–3268.
[41] M.R. Garcia-Cruz, A. Postma, J.E. Frith, L. Meagher, Printability and bio-functionality of a shear thinning methacrylated xanthan-gelatin composite bioink, Biofabrication 13 (2021).
[42] X. Li, Q. Sun, Q. Li, N. Kawazoe, G. Chen, Functional hydrogels with tunable structures and properties for tissue engineering applications, Front. Chem. 6 (2018).
[43] J. Zhang, J. Guan, C. Zhang, H. Wang, W. Huang, S. Guo, X. Niu, Z. Xie, Y. Wang, Bioactive borate glass promotes the repair of radius segmental bone defects by enhancing the osteogenic differentiation of BMSCs, Biomed. Mater. 10 (2015), 65011.
[44] X. Cui, Y. Zhang, J. Wang, C. Huang, Y. Wang, H. Yang, W. Liu, T. Wang, D. Wang, G. Wang, C. Ruan, D. Chen, W.W. Lu, W. Huang, M.N. Rahaman, H. Pan, Strontium modulates osteogenic activity of bone cement composed of bioactive borosilicate glass particles by activating Wnt/beta-catenin signaling pathway, Bioact. Mater. 5 (2020) 334–347.
[45] F. Wei, M. Li, R. Crawford, Y. Zhou, Y. Xiao, Exosome-integrated titanium oxide nanotubes for targeted bone regeneration, Acta Biomater. 86 (2019) 480–492.
[46] J. Peng, J. Zhao, Q. Tang, J. Wang, W. Song, X. Lu, X. Huang, G. Chen, W. Zheng, L. Zhang, Y. Han, C. Yan, Q. Wan, L. Chen, Low intensity near-infrared light promotes bone regeneration via circadian clock protein cryptochrome 1, Int. J. Oral Sci. 14 (2022).
[47] S. Wang, G. Huang, Y. Dong, Directional migration and odontogenic differentiation of bone marrow stem cells induced by dentin coated with nanobioactive glass, J. Endodont 46 (2020) 216–223.
[48] C. Shen, P. Lie, T. Miao, M. Yu, Q. Lu, T. Feng, J. Li, T. Zu, X. Liu, H. Li, Conditioned medium from umbilical cord mesenchymal stem cells induces migration and angiogenesis, Mol. Med. Rep. 12 (2015) 20–30.
[49] K. Hu, B.R. Olsen, Osteoblast-derived VEGF regulates osteoblast differentiation and bone formation during bone repair, J. Clin. Invest. 126 (2016) 509–526.
[50] T. Ding, W. Kang, J. Li, L. Yu, S. Ge, An in situ tissue engineering scaffold with growth factors combining angiogenesis and osteoimmunomodulatory functions for advanced periodontal bone regeneration, J. Nanobiotechnol. 19 (2021).
[51] Q. Qin, S. Lee, N. Patel, K. Walden, M. Gomez-Salazar, B. Levi, A.W. James, Neurovascular coupling in bone regeneration, Exp. Mol. Med. 54 (2022) 1844–1849.
[52] J. Cui, X. Yu, B. Yu, X. Yang, Z. Fu, J. Wan, M. Zhu, X. Wang, K. Lin, Coaxially fabricated dual-drug loading electrospinning fibrous mat with programmed releasing behavior to boost vascularized bone regeneration, Adv. Healthc. Mater. 11 (2022), e2200571.
[53] H. Xu, Y. Zhu, A.W. Hsiao, J. Xu, W. Tong, L. Chang, X. Zhang, Y. Chen, J. Li, W. Chen, Y. Zhang, H.F. Chan, C. Lee, Bioactive Glass-Elicited Stem Cell-Derived Extracellular Vesicles Regulate M2 Macrophage Polarization and Angiogenesis to Improve Tendon Regeneration and Functional Recovery, BIOMATERIALS, 2023, p. 294.
[54] H. Shen, J. Liu, X. Yan, H. Yang, S. Hu, X. Yan, T. Xu, A.J.E. Haj, Y. Yang, L. Lue, Hydrostatic Pressure Stimulates the Osteogenesis and Angiogenesis of MSCs/HUVECs Co-culture on Porous PLGA Scaffolds, vol. 213, COLLOID SURFACE B, 2022.
[55] C. Piard, A. Jeyaram, Y. Liu, J. Caccamese, S.M. Jay, Y. Chen, J. Fisher, 3D printed HUVECs/MSCs cocultures impact cellular interactions and angiogenesis depending on cell-cell distance, Biomaterials 222 (2019), 119423.
[56] L. Li, M. Yu, Y. Li, Q. Li, H. Yang, M. Zheng, Y. Han, Di Lu, S. Lu, L. Gui, Synergistic anti-inflammatory and osteogenic n-HA/resveratrol/chitosan composite microspheres for osteoporotic bone regeneration, Bioact. Mater. 6 (2021) 1255–1266.
[57] Z. Yuan, X. Yuan, Y. Zhao, Q. Cai, Y. Wang, R. Luo, S. Yu, Y. Wang, J. Han, L. Ge, J. Huang, C. Xiong, Injectable GelMA cryogel microspheres for modularized cell delivery and potential vascularized bone regeneration, Small 17 (2021).
[58] J.H. Hwang, Y.S. Park, H.S. Kim, D. Kim, S.H. Lee, C.H. Lee, S.H. Lee, J.E. Kim, S. Lee, H.M. Kim, H.W. Kim, J. Kim, W. Seo, H.J. Kwon, B.J. Song, D.K. Kim, M. C. Baek, Y.E. Cho, Yam-derived exosome-like nanovesicles stimulate osteoblast formation and prevent osteoporosis in mice, J. Control Release 355 (2023) 184–198.
[59] S.S. Jin, D.Q. He, D. Luo, Y. Wang, M. Yu, B. Guan, Y. Fu, Z.X. Li, T. Zhang, Y. H. Zhou, C.Y. Wang, Y. Liu, A biomimetic hierarchical nanointerface orchestrates macrophage polarization and mesenchymal stem cell recruitment to promote endogenous bone regeneration, ACS Nano 13 (2019) 6581–6595.